energies

MDPI

Article

Vector Modulation-Based Model Predictive Current Control with Filter Resonance Suppression and Zero-Current Switching Sequence for Two-Stage Matrix Converter

Zhengfei Di *, Demin Xu and Kehan Zhang *

State Key Laboratory of Underwater Information and Control, Northwestern Polytechnical University, Xi'an 710072, China; xudm@nwpu.edu.cn

* Correspondence: dizhengfei2007@126.com (Z.D.); zhangkehan210@163.com (K.Z.)

Abstract: This paper proposes a novel model predictive current control scheme for two-stage matrix converter. The switching frequency is kept constant by fixing the switching instant. The control strategy achieves to control source reactive power in the input side and output currents in the output side. In addition, the advantage of the proposed strategy compared with conventional model predictive control is firstly proved using the principle of vector synthesis and the law of sines in the vector distribution area. Moreover, a zero-current switching sequence is proposed and implemented to insure zero-current switching operations and reduce the switching losses. Furthermore, in order to suppress the input filter resonance, which is easier to be inspired by the model predictive control, compared with traditional control strategies, an innovative active damping technique is proposed and implemented. Finally, both simulation and experiment are implemented to verify the performance of the proposed strategy. The results demonstrate that the control system features both good steady and transient performance.

Keywords: two-stage matrix converter; model predictive control; vector synthesis; zero-current switching strategy; input filter resonance suppression

Citation: Di, Z.; Xu, D.; Zhang, K. Vector Modulation-Based Model Predictive Current Control with Filter Resonance Suppression and Zero-Current Switching Sequence for Two-Stage Matrix Converter. *Energies* **2021**, *14*, 3685. https://doi.org/10.3390/en14123685

Academic Editor: Elyas Rakhshani

Received: 10 May 2021
Accepted: 15 June 2021
Published: 21 June 2021

1. Introduction

Matrix converters (MC) can offer direct AC–AC power conversion with no use of DC-link capacitors and have often been studied as an alternative to the traditional power topologies [1,2]. The most known MC topologies are named one-stage matrix converter (OSMC) and two-stage matrix converter (TSMC), which have the same transfer function [3,4]. The converter family has been globally discussed in all respects of control schemes, power topologies and trends in recent years [5–7]. The space vector modulation (SVM) method has been a mature technique for MC, in which both the input and output voltages and currents are considered using space vectors [8–11], whereas model predictive control (MPC) defies SVM with the emergence of developing digital processors and power devices [12–14]. MPC predicts and optimizes MC's future behaviors by minimizing a user-defined and model-based cost function and features several advantages such as simpler modifications, tuning and implementation of the control algorithm in modern digital control platforms [15–17].

However, due to the lack of modulation schemes, the conventional MPC (CMPC) optimizes and applies only one optimal switching state in the sampling period; the selected one optimal switching state probably leads to the minimum errors in more than one sampling periods, which results in a variable switching frequency and produces a broad harmonic spectrum [18]. On the contrary, traditional linear pulse width modulation (PWM) schemes can concentrate the harmonic spectrum around the carrier frequency and its multiples. Owing to this, in spite of the fast dynamic response of the CMPC, the performance in the steady state is usually poorer than traditional linear PWM schemes with a suitable

proportion integration (PI) controller [19]. In addition, the variable switching frequency produced by the CMPC increases the difficulty in designing input filter parameters, since the input filter resonance is easier to be inspired [20]. In order to solve these problems, several attempts have been discussed in [18–26], where a modulation scheme is added into the CMPC. In [18], the multi-objective modulated model predictive control (M^2PC) was proposed and tested, where the ac current and the dc-link voltage are controlled in a grid-connected seven-level three-phase cascaded H-bridge back-to-back converter. The duty cycles are calculated with the cost function values of two adjacent states. A similar modulation scheme was introduced to the OSMC in [19,20], but only load current was controlled and the supply current was ignored, which is an important control objective for an MC. In [21], two enhanced predictive current control schemes with fixed switching frequency for the three-wire cascaded H-bridge converter were compared in terms of current tracking errors, power ripples and the grid current total harmonic distortion (THD), but no significantly better performance were obtained in both two methods. In [22], M^2PC was applied to a two-Level voltage source inverter. The switching frequency was kept constant by incorporating modulation of the current vectors in the predictive current control. Particularly, the optimized response was extended to the overmodulation region. In [23], M^2PC was introduced to modular multilevel converter, the duty cycles of the three selected vectors were calculated by the multiple current tracking errors minimization and one drawback of this was the large amount of calculation, due to the large number of active vectors utilized in the modular multilevel converter. In [24], a CMPC involving virtual space vectors was proposed for an ac–dc matrix converter. This method employs several virtual space vectors to without increasing sampling frequency. The same problem is the increased calculation amount. As mentioned in [18–24], several attempts have been implemented in several power converters, i.e., back-to-back converters (B2B), OSMCs, voltage source inverters (VSI), modular multilevel converters (MMC) and ac–dc matrix converter (ADC). However, few schemes have been discussed to apply to TSMCs. In [25], a M^2PC scheme with reduced common-mode voltage (CMV) was proposed to TSMC, the source reactive power was omitted, which is an important control objective for an MC. In addition, no experiment verification was involved in this article. In [26], three new strategies of typical M^2PC for reducing CMV were proposed for TSMC. From the simulation results, although the CMV was reduced, the waveforms of output currents were affected. In addition, the schemes still need to be verified by the experiment.

For matrix converters, an input filter is necessary for the commutation of switching devices and to mitigate against line-current harmonics. However, the filter configuration presents a resonance frequency and can be excited by the utility due to the potential fifth and seventh harmonics in the ac source (series resonance) and also by the converter itself (parallel resonance). In addition, the input filter resonance is easier to be inspired by the model predictive control, when compared with traditional control methods, leading to highly distorted line-side currents, which are also reflected in the load side because of the direct topology [26–33]. To improve this, one general passive damping method was realized by a damping resistor in parallel with the filter inductor, which is easy to implement. However, current flows through the resistor, leading to power loss and less attenuation around switching frequency [26]. In addition, the resistor cannot be used in some specific applications, such as the situation of a generator source where stator inductance acts as the filter inductor [27]. To overcome these problems, some active damping methods have been introduced and applied, which could suppress the oscillations effectively through algorithms without a physical resistor [28–33]. In [28], an active damping method was realized by adding the filtered capacitor voltages into input current references, which is strictly limited by assuming the independent control of input currents. In [29], an iterative design method is proposed to decide the filter parameters in consideration of the most significant grid-current harmonics, using a PWM strategy. In [30], another new active damping method is carried out by modifying input reference currents, which is based on SVM and not applicable to the predictive control where the input current reference is not

required. In [31–33], digital dc blockers are still applied to filter the capacitor voltages, even when the source voltages and source currents are also available, which worsen the dynamic performance and even could limit the range of parameter adjustment.

To solve these problems above, this paper proposes a novel model predictive control scheme for the TSMC. The main contributions of this paper are as follows:

1. A vector modulation-based model predictive current control (VMMPCC) strategy is proposed, which features the controllable source reactive power and the controllable output currents with fixed switching frequency output waveforms. The comparison between the proposed VMMPCC and existing methods is shown in Table 1.
2. The advantage of the VMMPCC strategy compared with the CMPC is firstly proved using the principle of vector synthesis and the law of sines in the vector distribution area.
3. A zero-current switching sequence (ZSS) is proposed, which can guarantee safe zero-current switching operations and reduce the switching losses. This pattern can simplify the commutation of the TSMC and avoid complex commutation strategies (e.g., four-step commutation) in traditional control methods.
4. A novel input filter resonance suppression (IFRS) method is proposed and applied in the VMMPCC for the TSMC, featuring good damping performance and easy implementation.

Table 1. Comparison between the proposed VMMPCC and existing methods.

Method	Switching Frequency	Design of the Input Filter	Computational Burden	Control Objective	Verification	Applications
The proposed VMMPCC	Fixed	common	common	Source reactive power and output currents	Simulation and experiment	TSMC
CMPC in [12–17]	Variable	difficult	common	Currents, voltages, power	Simulation and experiment	Many power converters
M^2PC in [18–24]	Fixed	common	Common [18–22], High [23,24]	Currents, lack of Source reactive power control	Simulation and experiment	B2B, VSI, MMC, ADC, OSMC
M^2PC in [25,26]	Fixed	common	common	Currents, lack of Source reactive power control	Simulation	TSMC

2. TSMC Mathematical System Model

The power circuit of the TSMC system is demonstrated in Figure 1. The TSMC is divided into the inverter stage and the rectifier stage.

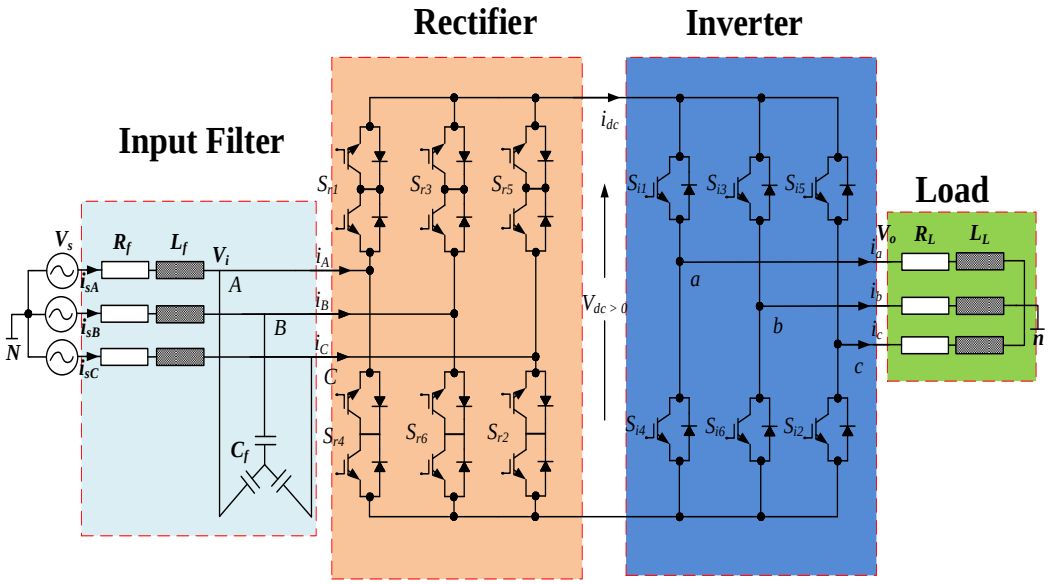

Figure 1. Power circuit of the TSMC system.

For the rectifier stage, the relationship between V_{dc} and V_i is [2]:

$$V_{dc} = \begin{bmatrix} S_{r1} - S_{r4} & S_{r3} - S_{r6} & S_{r5} - S_{r2} \end{bmatrix} V_i \tag{1}$$

$$S_{ri} = \begin{cases} 0, \text{open state} \\ 1, \text{closed state} \end{cases} \tag{2}$$

where $S_{ri}\{i \in (1,2,3,4,5,6)\}$ are the rectifier switching functions. In addition, the relationship between the input currents i_i and the dc-link current i_{dc} is [2]:

$$i_i = \begin{bmatrix} S_{r1} - S_{r4} \\ S_{r3} - S_{r6} \\ S_{r5} - S_{r2} \end{bmatrix} i_{dc} \tag{3}$$

The relationship between i_{dc} and i_o for the inverter stage is:

$$i_{dc} = \begin{bmatrix} S_{i1} - S_{i4} & S_{i3} - S_{i6} & S_{i5} - S_{i2} \end{bmatrix} i_o \tag{4}$$

$$S_{ix} = \begin{cases} 0, \text{open state} \\ 1, \text{closed state} \end{cases} \tag{5}$$

where $S_{ix}\{x \in (1,2,3,4,5,6)\}$ are the inverter switching functions. In addition, the relationship between the output voltage V_o and the dc-link voltage V_{dc} is [2]:

$$V_o = \begin{bmatrix} S_{i1} - S_{i4} \\ S_{i3} - S_{i6} \\ S_{i5} - S_{i2} \end{bmatrix} V_{dc} \tag{6}$$

All the valid switching states are shown in Tables 2 and 3.

In addition, an input filter is necessary to prevent over-voltages and harmonics and its model can be described as [2]:

$$\begin{cases} \frac{di_s}{dt} = \frac{1}{L_f}(V_s - V_i) - \frac{R_f}{L_f} i_s \\ \frac{dV_i}{dt} = \frac{1}{C_f}(i_s - i_i) \end{cases} \tag{7}$$

Similarly, the mathematical model in the load side is described as [2]:

$$V_o = L_L \frac{di_o}{dt} + R_L i_o \tag{8}$$

Table 2. Valid switching states of the rectifier.

V_{dc}	i_A	i_B	i_C	S_{r1}	S_{r2}	S_{r3}	S_{r4}	S_{r5}	S_{r6}
V_{AC}	i_{dc}	0	$-i_{dc}$	1	1	0	0	0	0
V_{BC}	0	i_{dc}	$-i_{dc}$	0	1	1	0	0	0
$-V_{AB}$	$-i_{dc}$	i_{dc}	0	0	0	1	1	0	0
$-V_{AC}$	$-i_{dc}$	0	i_{dc}	0	0	0	1	1	0
$-V_{BC}$	0	$-i_{dc}$	i_{dc}	0	0	0	0	1	1
V_{AB}	i_{dc}	$-i_{dc}$	0	1	0	0	0	0	1

Table 3. Valid switching states of the inverter.

i_{dc}	V_{ab}	V_{bc}	V_{ca}	S_{i1}	S_{i2}	S_{i3}	S_{i4}	S_{i5}	S_{i6}
i_a	V_{dc}	0	$-V_{dc}$	1	1	0	0	0	1
$i_a + i_b$	0	V_{dc}	$-V_{dc}$	1	1	1	0	0	0
i_b	$-V_{dc}$	V_{dc}	0	0	1	1	1	0	0
$i_b + i_c$	$-V_{dc}$	0	V_{dc}	0	0	1	1	1	0
i_c	0	$-V_{dc}$	V_{dc}	0	0	0	1	1	1
$i_a + i_c$	V_{dc}	$-V_{dc}$	0	1	0	0	0	1	1
0	0	0	0	1	0	1	0	1	0
0	0	0	0	0	1	0	1	0	1

3. Vector Modulation Based Model Predictive Control Strategy with Zero-Current Switching Sequence

The block diagram of the VMMPCC with the ZSS and the IFRS for the TSMC system is shown in Figure 2, including output current prediction, source reactive power prediction, cost function, the IFRS and the ZSS.

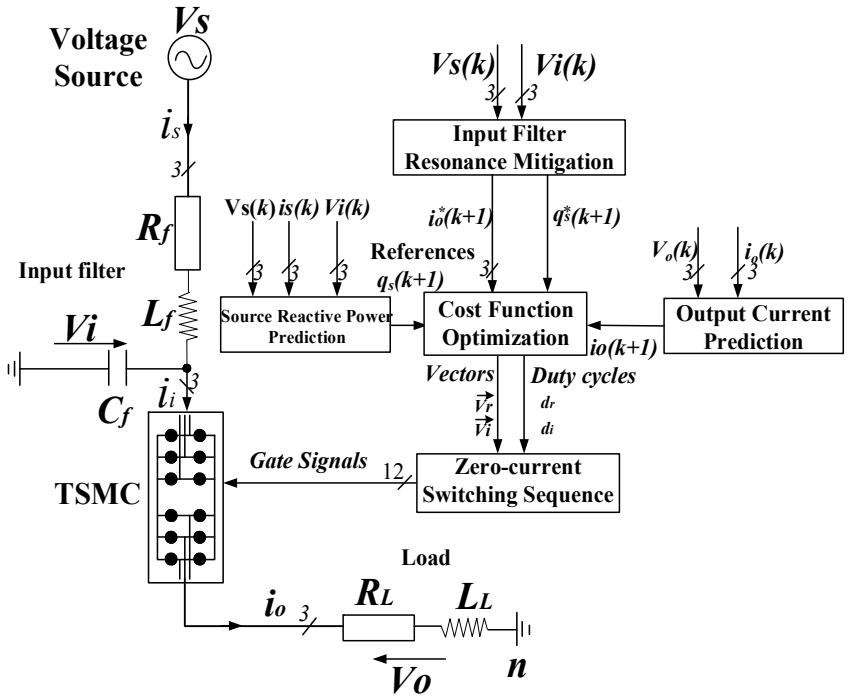

Figure 2. Block diagram of the VMMPCC with the ZSS and the IFRS.

Firstly, the IFRS generates the modified source reactive power reference $q_s^*(k+1)$ and output-current reference $i_o^*(k+1)$, then the output current prediction and the source reactive power prediction calculate $i_o(k+1)$, $q_s(k+1)$, which are the predicted values in the $(k+1)^{\text{th}}$ sampling period.

Secondly, with $i_o^*(k+1)$ and $q_s^*(k+1)$, the cost function selects the optimal switching states, which tracks their references at the end of the $(k+1)^{\text{th}}$ sampling instant.

Finally, in order to ensure safe zero-current switching operations, the proposed control strategy employs the ZSS scheme, in which the vectors are arranged in a symmetrical manner. The proposed control strategy is introduced in the following subsections.

3.1. Source Reactive Power Prediction and Output Current Prediction

The discrete model of input filter is [7,8]:

$$\begin{gathered}\begin{bmatrix} i_s(k+1) \\ V_i(k+1) \end{bmatrix} = \Phi_i \begin{bmatrix} i_s(k) \\ V_i(k) \end{bmatrix} + \Gamma_i \begin{bmatrix} V_s(k) \\ i_i(k) \end{bmatrix} \\ A_i = \begin{bmatrix} -R_f/L_f & -1/L_f \\ 1/C_f & 0 \end{bmatrix}, B_i = \begin{bmatrix} 1/L_f & 0 \\ 0 & -1/C_f \end{bmatrix}\end{gathered} \tag{9}$$

where $\Phi_i = e^{A_i T_s}$, $\Gamma_i = A_i^{-1}(\Phi_i - I)B_i$, R_f, L_f and C_f are the parameters of the input filter, T_s is the sampling time.

$q_s(k+1)$ can be expressed as:

$$q_s(k+1) = v_{s\alpha}(k+1)i_{s\beta}(k+1) - v_{s\beta}(k+1)i_{s\alpha}(k+1) \tag{10}$$

where $i_{s\alpha}(k+1)$, $i_{s\beta}(k+1)$ are the predicted source current and $v_{s\alpha}(k+1)$, $v_{s\beta}(k+1)$ represent the source voltage in the $(k+1)^{\text{th}}$ sampling period in $\alpha\beta$ reference frame.

Similarly, for the load stage, the discrete state-space model is calculated as [7,8]:

$$i_o(k+1) = \Phi_o i_o(k) + \Gamma_o V_o(k) \tag{11}$$

where L_L and R_L are the load inductance and resistance, $\Phi_o = e^{-\frac{R_L}{L_L}T_s}$, $\Gamma_o = -\frac{1}{R_L}(\Phi_o - 1)$.

3.2. Cost Function Optimization

For the inverter stage, six active vectors and two zero vectors are valid as shown in Figure 3a and associated with switching states in Table 3. The VMMPCC strategy uses two adjacent vectors V_{i1}, V_{i2} and one zero vector V_{i0}.

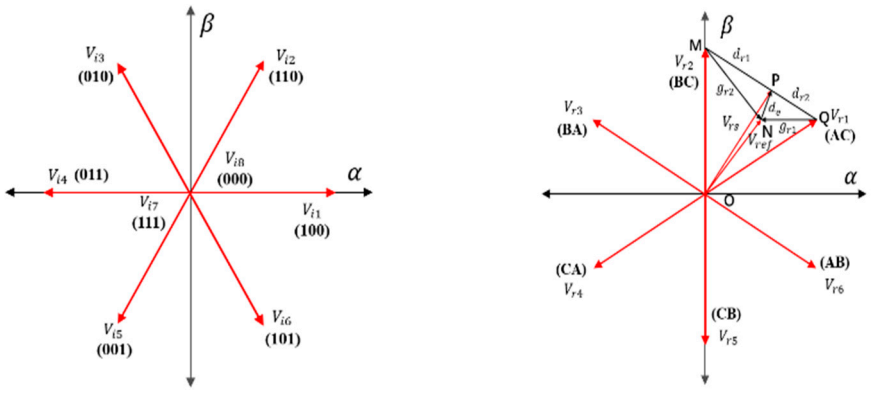

(**a**) (**b**)

Figure 3. Space vectors of the TSMC: (**a**) The inverter. (**b**) The rectifier.

Since the fundamental frequency is much lower than the sampling frequency and, thus, the control objective e_i error can be approximated as [18]:

$$e_i = \{d_{ij}e_{ij}\} \tag{12}$$

where e_{ij} represents the error when only vector $V_{ij}\{j \in (0,1,2)\}$ is applied for the whole sampling period T_s and d_{ij} is the duty cycle of V_{ij}.

Define e_{iRMS} as the root mean square (RMS) value of all the weighted errors, which can be calculated as [18]:

$$e_{iRMS} = \sqrt{\frac{\sum_{j=0}^{2}(d_{ij}e_{ij})^2}{3}} \tag{13}$$

and the mean value of the weighted errors is defined as [18]:

$$\overline{e_i} = \frac{1}{3}\sum_{j=0}^{2}(d_{ij}e_{ij}) \tag{14}$$

Since that $d_{ij}e_{ij} \geq 0$, minimizing e_i yields minimum values of $\overline{e_i}$ and e_{iRMS}. On this basis, the duty cycles can be obtained based on minimizing (13) as

$$min_{d_i}G_i = \frac{1}{3}\sum_{j=0}^{2}(d_{ij}e_{ij})^2 = \frac{1}{3}\sum_{j=0}^{2}g_{ij}(d_{ij})^2 \tag{15}$$

$$\sum_{j=0}^{2}d_{ij} = 1, (0 \leq d_{ij} \leq 1) \tag{16}$$

This optimization problem could be solved using the Lagrange multipliers method. To find the stationary points of a function $f(x,y)$ subject to the constraint $g(x,y) = 0$, the Lagrangian function is defined as [23]:

$$L(x,y,\lambda) = f(x,y) + \lambda g(x,y) \tag{17}$$

Then, the optimization problem turns to minimization of (18):

$$f(d_{i0},d_{i1},d_{i2}) = \frac{1}{3}g_0d_{i0}^2 + \frac{1}{3}g_1d_{i1}^2 + \frac{1}{3}g_2d_{i2}^2 \tag{18}$$

$$g_i = (i_o^*(k+1) - i_o(k+1))^2 \tag{19}$$

In (18), d_{i0}, d_{i1}, d_{i2} are the duty cycles and $g_0,\ g_1,\ g_2$ represent the cost function values for three active vectors $V_{i0}, V_{i1},\ V_{i2}$. The constraint is

$$g(d_{i0},d_{i1},d_{i2}) = d_{i0} + d_{i1} + d_{i2} - 1 \tag{20}$$

Rewrite the Lagrangian function by substituting (18) and (20) into (17) as

$$L(d_{i0},d_{i1},d_{i2},\lambda) = \frac{1}{3}g_0d_{i0}^2 + \frac{1}{3}g_1d_{i1}^2 + \frac{1}{3}g_2d_{i2}^2 + \lambda(d_{i0} + d_{i1} + d_{i2} - 1) \tag{21}$$

Then, the gradient of $L(d_{i0},d_{i1},d_{i2},\lambda)$ can be obtained as

$$\nabla_{d_{i0},d_{i1},d_{i2},\lambda}L(d_{i0},d_{i1},d_{i2},\lambda) = \left(\frac{\partial L}{\partial d_{i0}}, \frac{\partial L}{\partial d_{i1}}, \frac{\partial L}{\partial d_{i2}}, \frac{\partial L}{\partial \lambda}\right) \tag{22}$$

Substitute (21) into (22)

$$\nabla_{d_{i0},d_{i1},d_{i2},\lambda} L(d_{i0},d_{i1},d_{i2},\lambda) = \left(\frac{2}{3}g_0 d_{i0} + \lambda,\ \frac{2}{3}g_1 d_{i1} + \lambda,\ \frac{2}{3}g_2 d_{i2} + \lambda,\ d_{i0} + d_{i1} + d_{i2} - 1\right) \tag{23}$$

Consider the minimization condition

$$\nabla_{d_{i0},d_{i1},d_{i2},\lambda} L(d_{i0},d_{i1},d_{i2},\lambda) = 0 \tag{24}$$

Combine (23) and (24), the duty cycles can be obtained as

$$\begin{cases} d_{i0} = \frac{g_1 g_2}{g_0 g_1 + g_0 g_2 + g_1 g_2} \\ d_{i1} = \frac{g_0 g_2}{g_0 g_1 + g_0 g_2 + g_1 g_2} \\ d_{i2} = \frac{g_0 g_1}{g_0 g_1 + g_0 g_2 + g_1 g_2} \end{cases} \tag{25}$$

$$\lambda = -\frac{2}{3}\frac{g_0 g_1 g_2}{g_0 g_1 + g_0 g_2 + g_1 g_2} \tag{26}$$

The total cost function g_i and the synthesized vector V_{is} can be expressed as follows:

$$g_i = d_{i0} g_{i0+} d_{i1} g_{i1} + d_{i2} g_{i2} \tag{27}$$

$$V_{is} = d_{i0} V_{i0+} d_{i1} V_{i1} + d_{i2} V_{i2} \tag{28}$$

In the similar way, six active vectors for the rectifier stage are considered as shown in Figure 3b, associated with switching states in Table 2. The VMMPCC strategy considers two valid adjacent vectors $V_{r1},\ V_{r2}$ and assesses two respective cost functions $g_{r1},\ g_{r2}$. The duty cycles $d_{r1},\ d_{r2}$ can be calculated as:

$$\begin{cases} d_{r1} = g_{r2}/(g_{r1} + g_{r2}) \\ d_{r2} = g_{r1}/(g_{r1} + g_{r2}) \\ d_{r1} + d_{r2} = 1 \end{cases} \tag{29}$$

$$g_r = (q_s^* - q_s(k+1))^2 \tag{30}$$

with $d_{r1},\ d_{r2}$, the total cost function g_r and the synthesized vector V_{rs} can be expressed as:

$$g_r = d_{r1} g_{r1} + d_{r2} g_{r2} \tag{31}$$

$$V_{rs} = d_{r1} V_{r1} + d_{r2} V_{r2} \tag{32}$$

3.3. Comparision between the Proposed VMMPCC and the CMPC

As shown in Figure 3b, the length of the segment NQ is g_{r1}, defined as the error when only the vector V_{r1} is applied and the length of the segment MN is g_{r2}, defined as the error when only the vector V_{r2} is applied, respectively.

From Equations (29)–(32), (33) and (34) can be obtained:

$$V_{rs} = V_{r2} + d_{r1}(V_{r1} - V_{r2}) \tag{33}$$

$$V_{rs} = V_{r1} + d_{r2}(V_{r2} - V_{r1}) \tag{34}$$

From Equations (33) and (34), obviously that the end point of V_{rs} (tagged as P) should be located on MQ and the length of MQ is d_{MQ}. In addition, the length of the segment MP is $d_{r1} d_{MQ}$ and the length of MP is $d_{r2} d_{MQ}$, respectively.

Consider Equations (29), (33) and (34) and the law of sines, (35) can be obtained:

$$\frac{\sin(\angle \mathrm{MNP})}{\sin(\angle \mathrm{MPN})} = \frac{d_{r1} d_{MQ}}{g_{r2}} = \frac{d_{r2} d_{MQ}}{g_{r1}} = \frac{\sin(\angle \mathrm{PNQ})}{\sin(\angle \mathrm{NPQ})} \tag{35}$$

Besides, since $\angle\mathrm{MPN} + \angle\mathrm{NPQ} = \pi$, thus, $\sin(\angle\mathrm{MPN}) = \sin(\angle\mathrm{NPQ})$, (36) can be obtained as:

$$\sin(\angle\mathrm{MNP}) = \sin(\angle\mathrm{PNQ}) \tag{36}$$

Consider two conditions based on (36):

1. $\angle\mathrm{MNP} + \angle\mathrm{PNQ} = \pi$; This means that P and Q are the same points and the error d_e between the synthesized vector V_{rs} and the reference vector V_{ref} (equal to the length of PN) is zero;
2. $\angle\mathrm{MNP} = \angle\mathrm{PNQ}$. In fact, since:

$$\begin{cases} \angle\mathrm{NQP} < \angle\mathrm{OQM} = \pi/3 \\ \angle\mathrm{NPQ} = \angle\mathrm{MNP} + \angle\mathrm{NMP} > \angle\mathrm{PNQ} \\ \angle\mathrm{PNQ} + \angle\mathrm{NPQ} = \pi - \angle\mathrm{NQP} > 2\pi/3 \end{cases} \tag{37}$$

Thus, $\angle\mathrm{NPQ} > \pi/3 > \angle\mathrm{NQP}$. $d_e < g_{r1}$ is obtained based on the law of sine. In the similar way, $d_e < g_{r2}$ is deduced. Both the two conditions verify the advantages of the VMMPCC strategy over the CMPC.

3.4. Zero-Current Switching Sequence

As can be seen in Figure 1, the rectifier stage connects the inverter stage directly. A zero-current switching sequence is proposed in this paper. The ZSS proposed is shown in Figure 4.

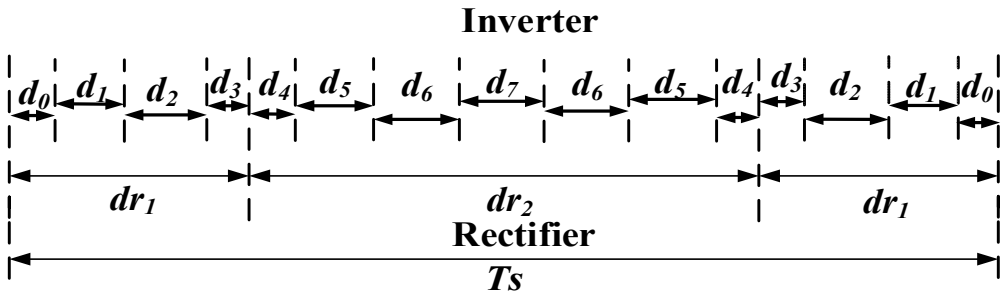

Figure 4. Zero-current switching sequence.

The duty cycles $d_0 \sim d_7$ for the inverter are calculated as:

$$\begin{cases} d_0 = d_3 = \frac{d_{i1}d_{i0}}{4} \\ d_1 = \frac{d_{i1}d_{r1}}{2} \\ d_2 = \frac{d_{i2}d_{r1}}{2} \\ d_4 = \frac{d_{i2}d_{i0}}{4} \\ d_5 = \frac{d_{i2}d_{r2}}{2} \\ d_6 = \frac{d_{i1}d_{r2}}{2} \\ d_7 = \frac{d_{i2}d_{i0}}{2} \end{cases} \tag{38}$$

Moreover, the duty cycles $d_{r1} \sim d_{r2}$ for the rectifier are

$$\begin{cases} d_{r1} = 2d_0 + d_1 + d_2 \\ d_{r2} = 2(d_4 + d_5 + d_6) + d_7 \end{cases} \tag{39}$$

Obviously, the rectifier state commutation always happens, when zero voltage vector is implemented for the inverter and $i_{dc} = 0$. Owing to this, zero-current switching operations and reduction of the switching losses of the TSMC are achieved, which can simplify the commutation strategy.

4. Input Filter Resonance Suppression

An active damping technique is crucial to the TSMC control system [26–33], as shown in Figure 5. Figure 5a shows the traditional active damping method 1 [26–30], which considers a virtual resistor R_{vd} placed in parallel with C_f. Figure 5b shows another active damping method 2 [31–33], the virtual branch is considered in parallel with C_f, consisting of a virtual resistor R_{vd} in series with a virtual capacitor C_{vd}. The main drawback of method 1 and method 2 is the limited effectiveness and applications. From Figure 5a,b, the damping current i_{vd} is obtained from the input voltage V_i, which contains fundamental frequency components and will affect the normal operations of the TSMC. In [31–33], dc blockers are stilled applied to filter the capacitor voltages, even when the source voltages and source currents are also available. The digital filters worsen the dynamic performance and even could limit the range of parameters adjustment. Figure 5c shows the proposed active damping method, the virtual branch consists of a virtual damping resistor R_{vd}, a virtual voltage source same as the source voltage V_s and an added item $\mathrm{j}\omega_s L_f I_s$, where ω_s denotes the source frequency and I_s represents the fundamental source current under steady state. I_s can be obtained based on instantaneous power theory [34].

$$I_s = (P_i^* + jQ_i^*)V_s / \|V_s\|^2 \tag{40}$$

and the damping current i_{vd} is expressed as:

$$i_{vd} = \frac{V_i - V_s + \mathrm{sj}\omega_s L_f I_s}{R_{vd}} \tag{41}$$

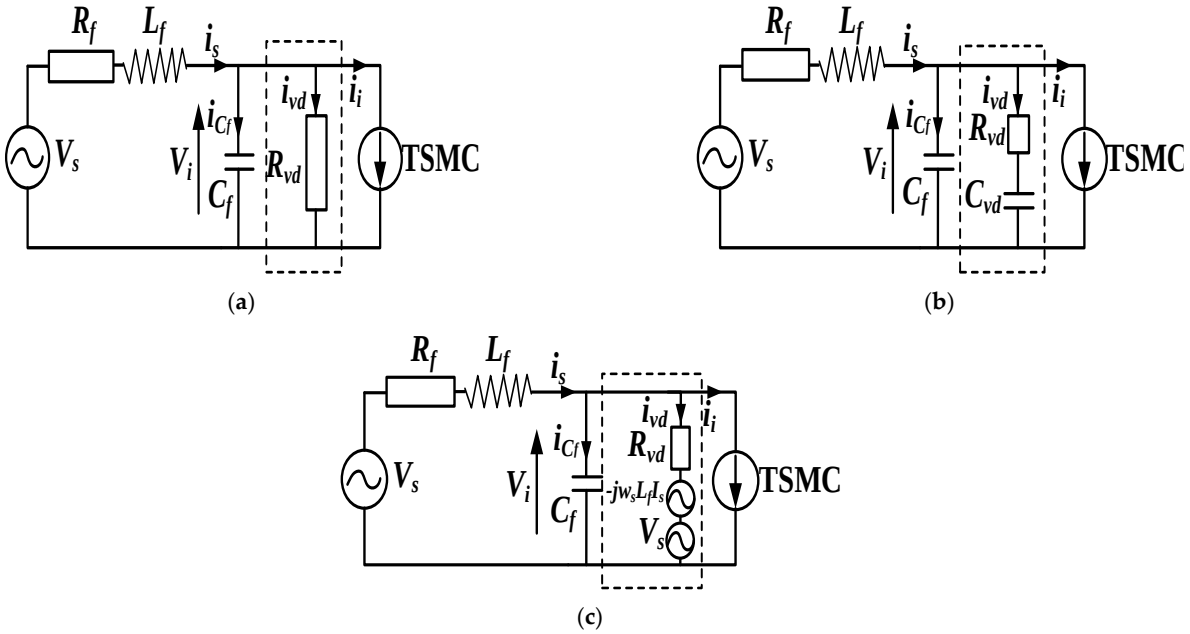

Figure 5. Different active damping methods: (**a**) The first method. (**b**) The second method. (**c**) The proposed method.

In (41), the items V_s and $\mathrm{sj}\omega_s L_f I_s$ contribute to remove the fundamental frequency component in i_{vd}, in such way i_{vd} will not affect the control accuracy and improve the effectiveness of active damping.

The small-signal transfer function from i_i to i_s can be expressed as:

$$\mathrm{G(s)} = \frac{1}{s^2 L_f C_f + s\left(L_f / R_{vd} + \left(1 + R_f / R_{vd}\right) C_f\right) + 1 + R_f / R_{vd}} \tag{42}$$

From Figure 6, it is obvious that when R_{vd} decreases, the damping coefficient increases. Meanwhile, the magnitude at high frequency does not change, which means the proposed IFRS method can achieve both good filtering and damping performance.

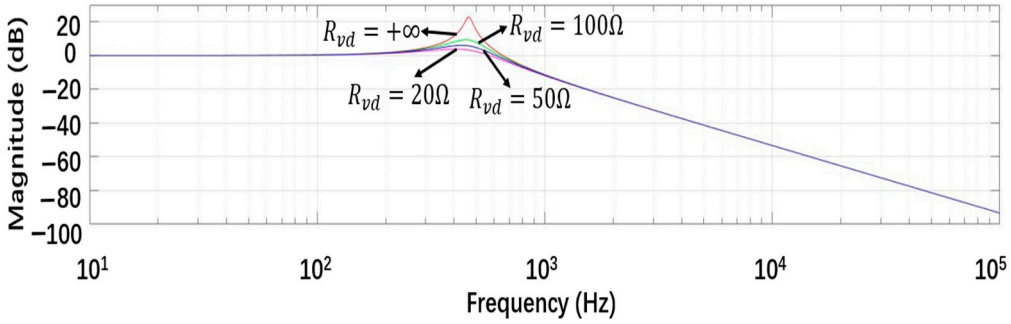

Figure 6. Spectrum of transfer function from the input current to the source current in the IFRS.

As shown in Figure 5c, the source current i_s is expressed as:

$$i_s = i_i + i_{C_f} + i_{vd} \tag{43}$$

Thus, the damping effect can be realized by modifying the reference value of i_s by injecting i_{vd}. However, rather than the source current i_s, the proposed VMMPCC strategy controls source reactive power and output currents directly (seen in Equations (19) and (30)). Hence, the input apparent power s_i can be obtained as:

$$s_i = V_i i_s^C = V_i\left(i_i^C + i_{C_f}^C\right) + V_i i_{vd}^C \tag{44}$$

From (44), the damping effect can be realized by injecting $V_i i_{vd}^C$ into the reference values of s_i. Therefore, the reference value of input active power p_i should be modified with the real part of $V_i i_{vd}^C$ and the reference value of reactive power q_i should be modified with the imaginary part of $V_i i_{vd}^C$, respectively,

$$p_i^* = P_i^* + Re(V_i i_{vd}^c) \tag{45}$$

$$q_i^* = Q_i^* + Im(V_i i_{vd}^c) \tag{46}$$

It should be noticed here, in this paper, that rather than the input active power p_i, the proposed VMMPCC strategy controls output currents directly. Thus, (45) cannot be applied directly. The relationship between the input active power p_i and output active power p_L is [12]:

$$p_i^* \eta = p_L^* = \frac{3}{2} R_L (I_o^*)^2 \tag{47}$$

where η represents the efficiency of the TSMC and I_o^* is the reference amplitude of output currents.

Thus, the reference amplitude of output currents i_o^* can be modified as shown in (48):

$$i_o^* = \sqrt{(I_o^*)^2 + \frac{2\eta Re\left(V_i i_{vd}^c\right)}{3R_L}} \tag{48}$$

In addition, the source reactive power q_s can be obtained as:

$$\begin{aligned} q_s = Im(V_s i_s^c) \quad &= Im\left[\left(V_i + R_f i_s + L_f \tfrac{di_s}{dt}\right) i_s^c\right] = Im\left(V_i i_s^c + L_f \tfrac{di_s}{dt} i_s^c\right) \\ &= q_i + L_f \tfrac{di_s}{dt} i_s^c \end{aligned} \tag{49}$$

From Equation (49), it is obvious that the difference between q_s and q_i is related to the voltage drop on L_f, which is negligible compared with V_s in a proper LC filter. Hence, q_i and q_s can be considered equal.

Finally, the IFRS is implemented by modifying the reference values i_o^* with the real part of $V_i i_{vd}^c$ and q_s^* with the imaginary part of $V_i i_{vd}^c$.

5. Simulation Results

To verify the proposed strategy, simulation has been done and the relevant parameters are demonstrated in Table 4.

Table 4. System parameters.

V_s	The amplitude of source voltage	141 V
L_f	Input filter inductor	5 mH
R_f	Input filter resistor	0.5 Ω
C_f	Input filter capacitor	21 μF
L_L	Load inductor	5 mH
R_L	Load resistor	5 Ω
T_s	Sampling time	100 μs
f_s	Sampling frequency	10 kHz

The input filter resonance can be excited by the utility (series resonance) due to the potential fifth and seventh harmonics in the AC source (seen in Figure 7a) and also by the converter itself (parallel resonance seen in Figure 7b). Normally, the filter resonant frequency is designed both one decade above the input supply frequency f_w and one decade below the switching frequency f_s to minimize the effect of the resonance introduced by the filter [35]. That is

$$10f_w < f_{res} = \frac{1}{2\pi\sqrt{LC}} < 10f_s \tag{50}$$

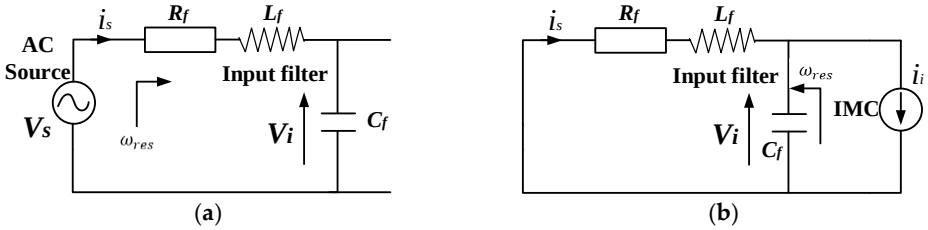

Figure 7. Possible input filter resonances. (**a**) Series resonance. (**b**) Parallel resonances.

In this paper, the resonant frequency is designed and situated nearly at the seventh harmonic of the source system to excite the resonant situation, in which the TSMC system performance can be compared with the IFRS and without the IFRS [35].

$$f_{res} = \frac{1}{2\pi\sqrt{LC}} \approx 7(\text{pu}) \tag{51}$$

As shown in Figure 8, the IFRS is added at 0.06 s. Before that, the source current is highly distorted due to the input filter resonance. After 0.06 s, obviously the source current is significantly improved and achieves a very good tracking to its reference. Besides, the output current shows an almost sinusoidal waveform and approaches its reference in Figure 8b. The results of another simulation group are shown in Figure 9, where the reference of the output-current frequency is changed to 25 Hz. As shown in Figures 8 and 9, the IFRS can greatly improve the quality of source current in spite of system reference variations. In addition, the source reactive power is minimized based on the Equations (10) and (30).

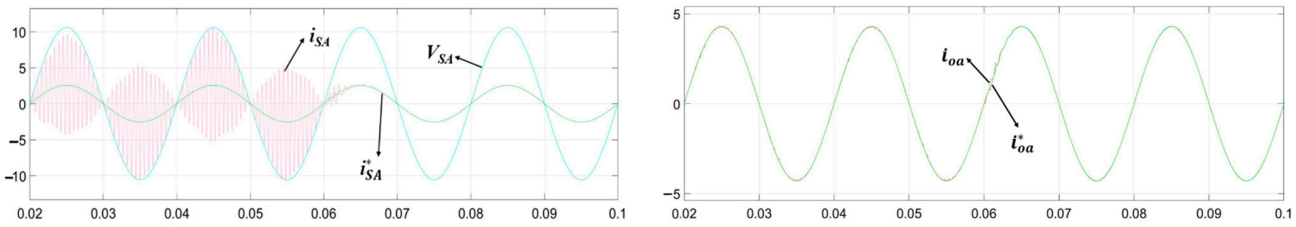

(**a**) (**b**)

Figure 8. Results of the VMMPCC for the TSMC and the reference of the output-current frequency is 50 Hz: The IFRS is added at t = 0.06 s, x axis unit second: (**a**) i_{sA}* A, i_{sA} A, V_{sA}/13 V; (**b**) i_{oa} A and i_{oa}* [A].

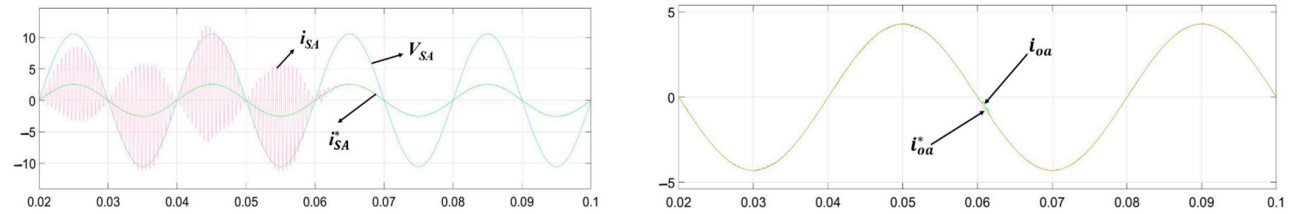

(**a**) (**b**)

Figure 9. Results of the VMMPCC for the TSMC and the reference of the output-current frequency is 25 Hz: The IFRS is added at t = 0.06 s, x axis unit second: (**a**) i_{sA}* A, i_{sA} A, V_{sA}/13 V; (**b**) i_{oa} A and i_{oa}* [A].

In order to verify the dynamic performance of the proposed VMMPCC strategy for the TSMC, two groups of simulation are implemented and the results are shown in Figures 10 and 11, considering the two conditions of with the IFRS and without the IFRS. In Figure 10, the output-current frequency steps from 25 Hz to 50 Hz. In Figure 11, the output-current reference amplitude steps from 4 A to 2 A. As shown in Figures 10b and 11b, the system resumes quickly after minute oscillations in a short time, when the output-current frequency or the output-current reference amplitude steps at t = 0.06 s. Besides, the output current and the source current still present good sinusoidal waveforms with the IFRS and the source reactive power is minimized, when the reference of the output-current amplitude and the reference of output-current frequency steps. At last, the control scheme presents a good dynamic performance in both input and output sides.

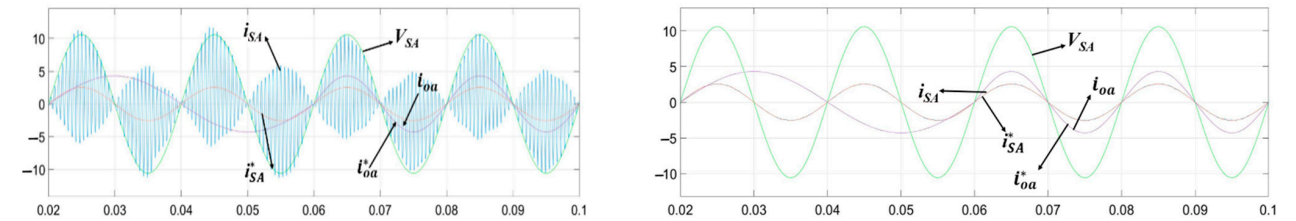

(**a**) (**b**)

Figure 10. Results of the VMMPCC for the TSMC and the reference of the output-current frequency steps from 25 Hz to 50 Hz at t = 0.06 s, V_{sA}/13 V, i_{sA}* A, i_{sA} A, i_{oa} A and i_{oa}* A, x axis unit second: (**a**) without the IFRS; (**b**) with the IFRS.

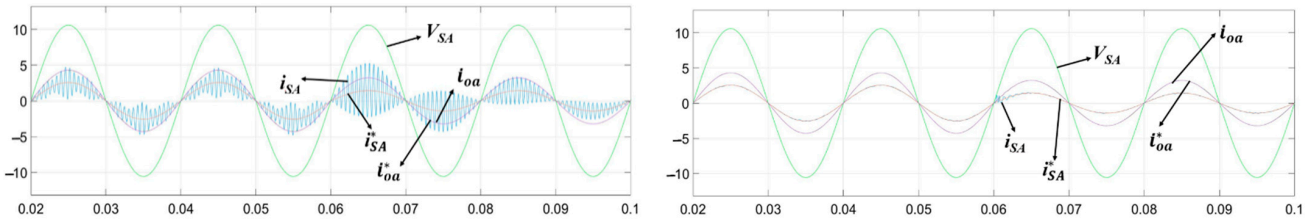

Figure 11. Results of the VMMPCC for the TSMC, in which the reference of the output-current amplitude steps from 4 A to 2 A at t = 0.06 s, V_{sA}/13 V, i_{sA}* A, i_{sA} A, i_{oa} A and i_{oa}* A, x axis unit second: (**a**) without the IFRS; (**b**) with the IFRS.

6. Experimental Results

To verify the proposed strategy, a laboratory prototype is designed and built for experimental evaluation. The prototype is shown in Figure 12 and the relevant experimental parameters are shown in Table 4. A digital control board integrating a ProASIC3 FPGA and a Texas Instruments C6713 DSP is used for the test and verification. Unlike the OSMC, where Silicon Carbide (SiC) MOSFETs are used for all the eighteen switches, this experiment use 12 standard insulated gate bipolar transistors (IGBT, IKW15T120) for the rectifier and six SiC MOSFETs (C2M0080120D) for the inverter, considering the high switching frequencies and the switching losses. In addition, a radiator is used to dissipate the heat produced by the high frequency switches. Moreover, the ac source output side connects an EMI filter, more details can be found in [36].

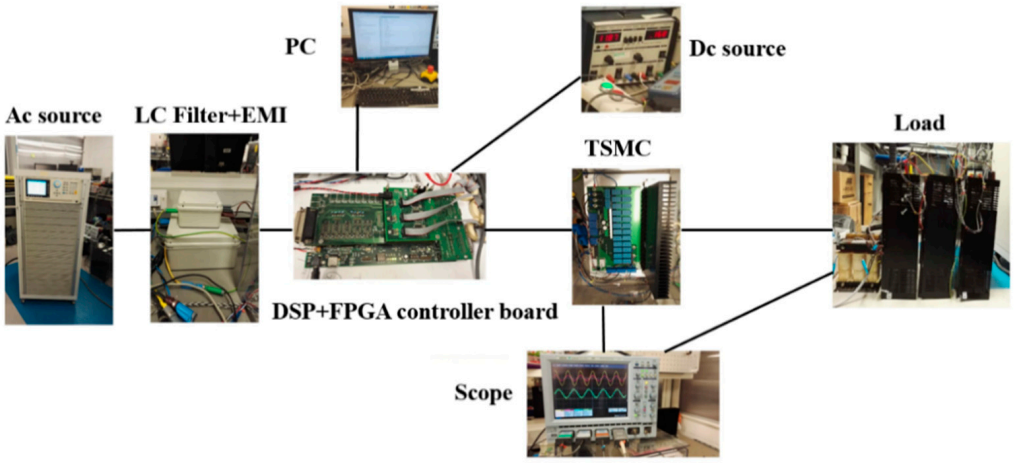

Figure 12. Laboratory TSMC system prototype for evaluation of the proposed control strategy.

Figure 13 shows the results of the conventional model predictive control strategy for the TSMC without the IFRS and the ZSS. From Figure 13, i_{sA} is highly distorted, mainly related to the input filter resonance. As seen in Figure 13b, the main distortions are situated around the input filter resonance frequency. Moreover, the waveforms of V_{sA} and i_{oa} are also affected by the large oscillations of i_s, due to the direct topology of the TSMC. From Figure 13, the input filter resonance is necessary to be suppressed to improve the power-quality performance of the TSMC system.

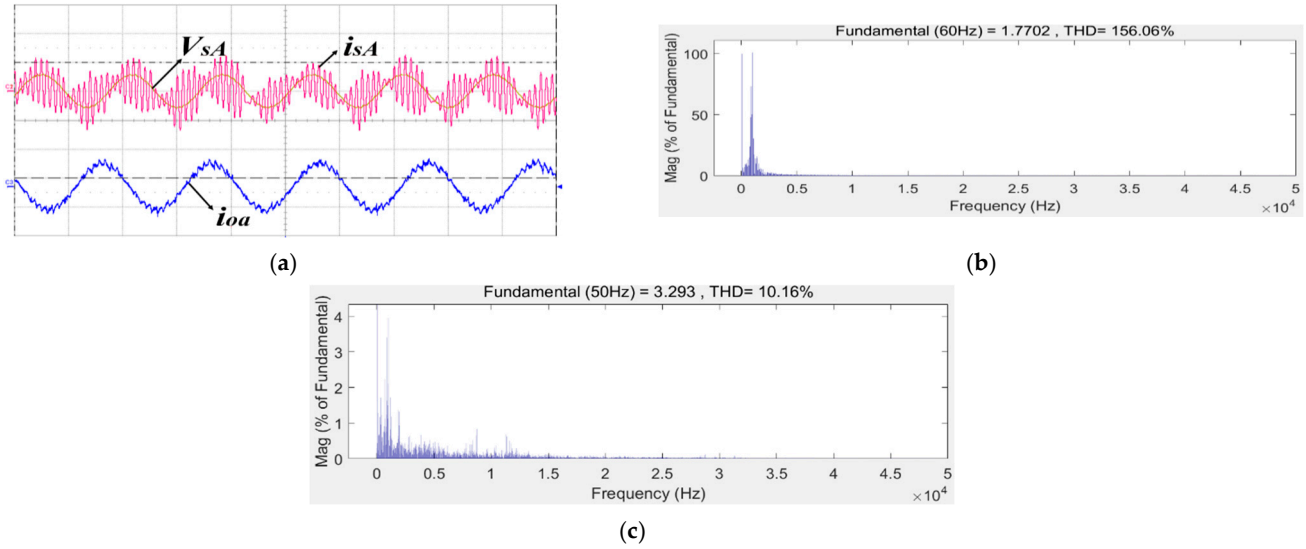

Figure 13. Experimental results of the CMPC without the IFRS for the TSMC: (**a**) Waveforms of source voltage V_{sA} (200 V/div), source current i_{sA} (2 A/div) and output current i_{oa} (5 A/div); (**b**) THD of i_{sA}; (**c**) THD of i_{oa}.

Figure 14 demonstrates the results of the situation, where the IFRS is added to the CMPC for the TSMC. Compared with Figure 13, with the help of the IFRS, the quality of i_{sA} is largely improved and the THD of the output current is also improved from 10.16% to 8.08% respectively. In addition, the variable switching frequency phenomenon can be easily observed in Figure 14b,c. In addition, i_{sA} is not always in phase with V_{sA} in Figure 14a, which indicates that the minimization of the instantaneous source reactive power based on Equations (10) and (30) need to be improved.

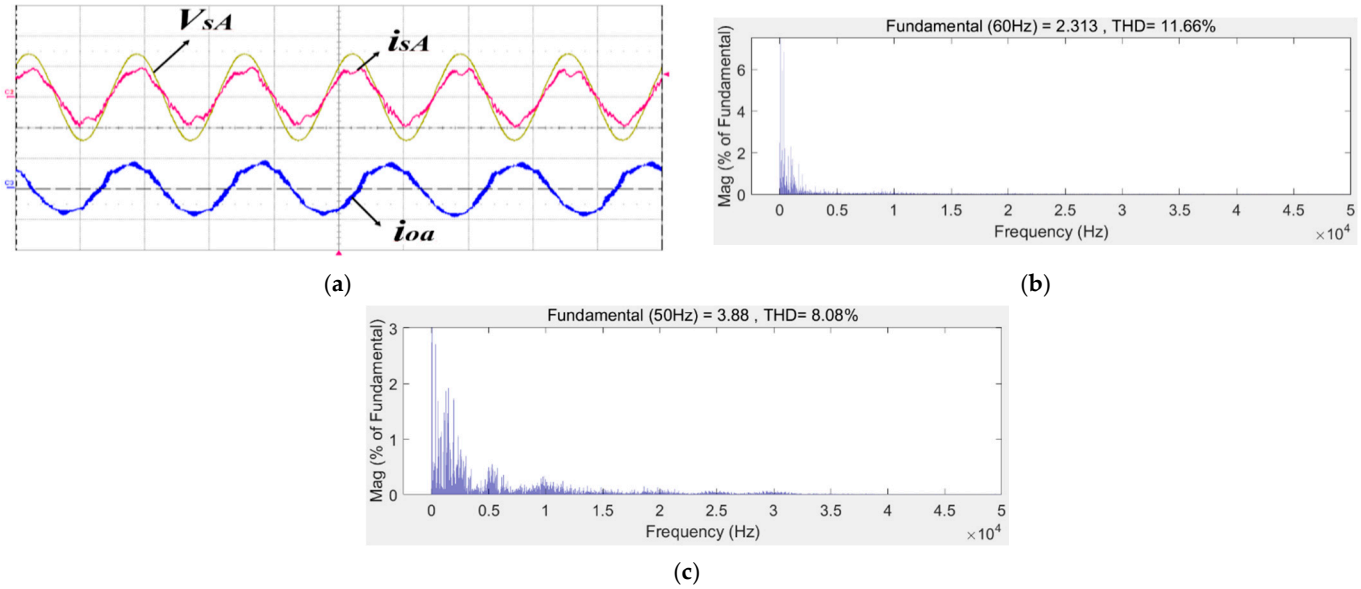

Figure 14. Experimental results of the CMPC with the IFRS for the TSMC, in which the reference of the output-current amplitude is 4 A and the reference of the output-current frequency is 50 Hz: (**a**) Waveforms of V_{sA} (100 V/div), i_{sA} (2 A/div) and i_{oa} (5 A/div); (**b**) THD of i_{sA}; (**c**) THD of i_{oa}.

Figure 15 shows the results of the proposed VMMPCC strategy with the IFRS and the ZSS. Compared with Figure 14a, the source current i_{sA} is improved with a THD from 11.66% to 7.44% and the THD of the output current is also improved from 8.08% to 6.55% respectively. In addition, the fixed switching frequency phenomenon can be easily observed in Figure 15b,c. In addition, i_{sA} is always in phase with V_{sA} in Figure 15a, which indicates

the minimization of the instantaneous source reactive power based on Equations (10) and (30) is also improved compared with Figure 14a.

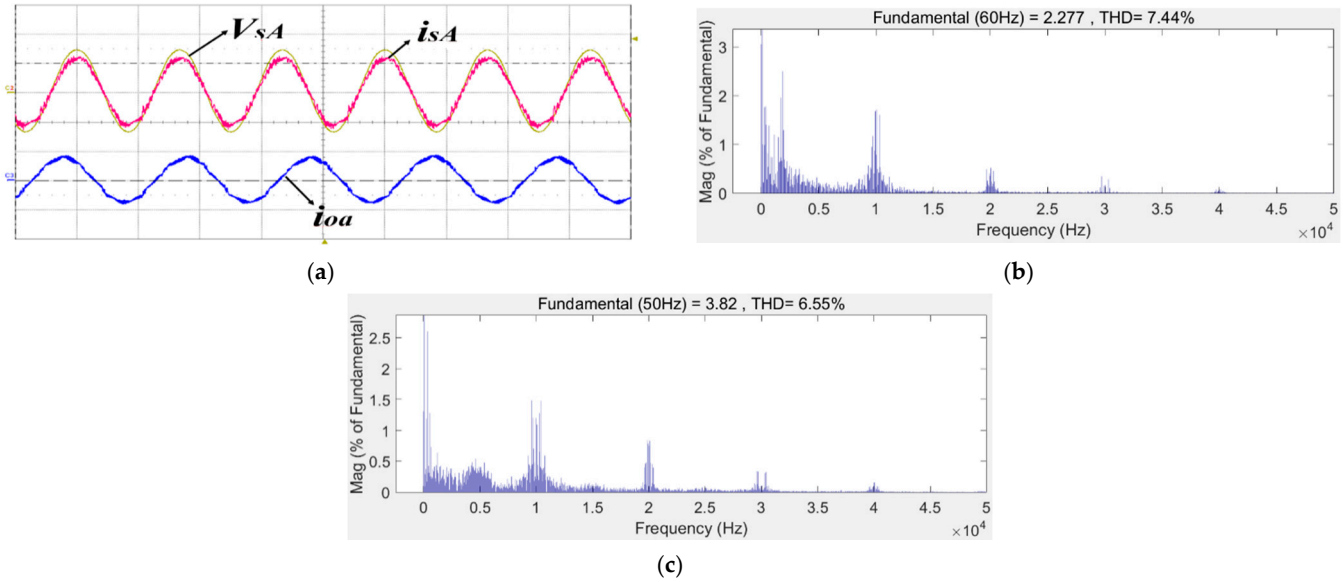

Figure 15. Experimental results of the proposed VMMPCC strategy with the IFRS and the ZSS for the TSMC, in which the reference of the output-current amplitude is 4 A and the reference of the output-current frequency is 50 Hz, x axis 10 ms/div (**a**) Waveforms of V_{sA} (100 V/div), i_{sA} (2 A/div) and i_{oa} (5 A/div). (**b**) Spectrum distribution of i_{sA}. (**c**) Spectrum distribution of i_{oa}.

The instantaneous source reactive power is controlled in the proposed control strategy in the input side, thus, the parameter named as the mean power M_p is defined to assess the performance [7]:

$$M_p = \frac{1}{m}\sum_{k=1}^{m}|p(k)| \tag{52}$$

In Equation (52), m is set to 10,000 and $p(k)$ is the actual value of power at the k^{th} sampling instant.

The comparisons between the CMPC and the proposed VMMPCC with the ZSS are shown in Table 5.

Table 5. The assessment parameters of experimental results.

Method	M_{q_s} (Var)	THD of i_s	THD of i_a
CMPC	9.37	11.66%	8.08%
VMMPCC	2.49	7.44%	6.55%

As shown in Table 5, the proposed VMMPCC with the ZSS can obtain better performance in all aspects of the instantaneous source reactive power, the source current and the output current, compared with the CMPC.

The CMPC may obtain the similar performance with the VMMPCC in aspects of control objectives, by using a much higher sampling frequency than that in the VMMPCC [18,24]. In fact, predictive controllers usually occupy the computational resources and, thus, the sampling frequency cannot always be increased in practical applications. In addition, the variable switching frequency with the CMPC is a lurking peril for the control system [31].

Besides, the amplitude of the output current is 3.82 A; thus, there exists a 4.5% steady state error, because that the reference of the output current is set to 4A. In fact, a steady state error between the measured current and its reference is normal in model-based control

strategies, where a steady-state error usually occurs from the system model inaccuracies. This can be usually compensated by external control loops (e.g., PI controller based). In addition, in [37], a method aiming to improve the system parameter robustness with the CPMC has been proposed, which can also mitigate this problem.

The waveforms of u_{dc} and i_{dc} with the CMPC and the VMMPCC with ZSS are demonstrated in Figure 16. The commutation of u_{dc} represents the change of the switching state for the rectifier stage. From Figure 16a, it is possible to change the switching state of the rectifier stage when i_{dc} is nonzero (green line), increasing the converter switching losses and requiring a complicated commutation strategy for the rectifier (e.g., four-step commutation). On the contrary, in Figure 16b with the proposed control strategy, the commutation of u_{dc} always occurs when i_{dc} is zero (green line), which guarantees the zero-current switching of the rectifier stage.

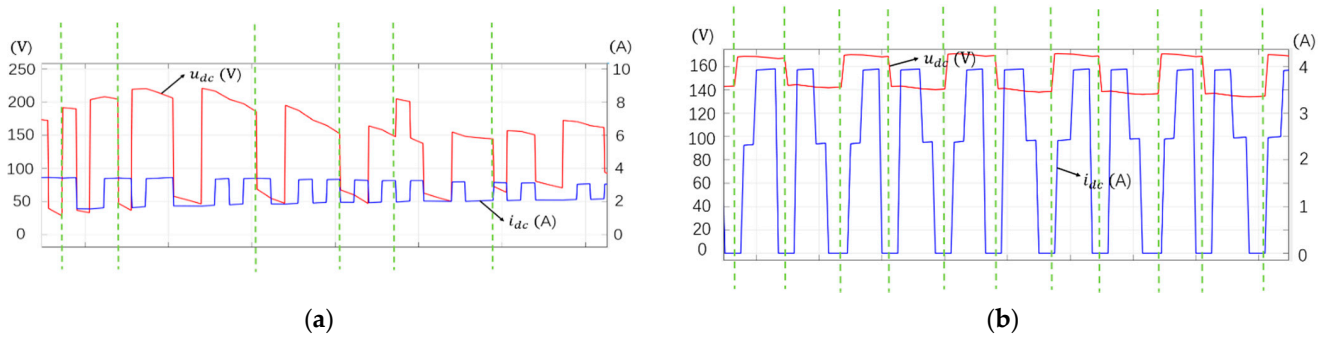

(**a**) (**b**)

Figure 16. u_{dc} and i_{dc}: (**a**) with the CMPC; (**b**) with the VMMPCC and the ZSS.

Figures 17–20 show the transient results of the proposed control strategy. The output-current frequency reference is changed between 25 Hz and 50 Hz in Figures 17 and 18 and its amplitude reference is changed between 2 A and 4 A in Figures 19 and 20. As indicated in Figures 17–20, almost sinusoidal waveforms of the source current and the output current are obtained and the output current shows a good tracking to the reference. In addition, the source current is in phase with the source voltage, achieving the minimization of the instantaneous source reactive power and the source and output currents show fast dynamic responses to the variations of the references. At last, the control scheme presents a good dynamic performance in both input and output sides.

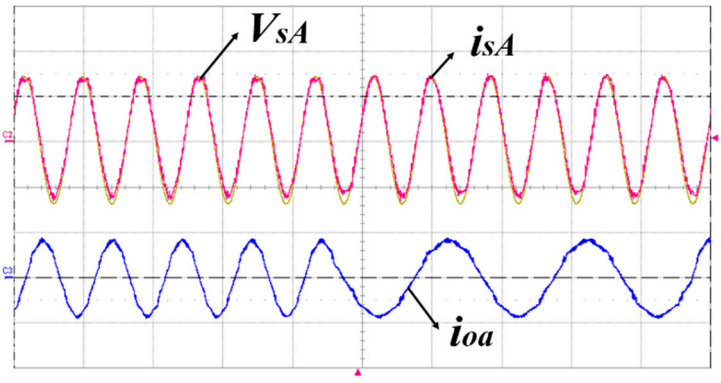

Figure 17. Experimental results of the proposed strategy with IFRS, in which the reference of the output-current amplitude is 4 A and the reference of the output-current frequency is changed from 50 Hz to 25 Hz, x axis 20 ms/div. Waveforms of source voltage V_{sA} (100 V/div), source current i_{sA} (2 A/div) and output current i_{oa} (5 A/div).

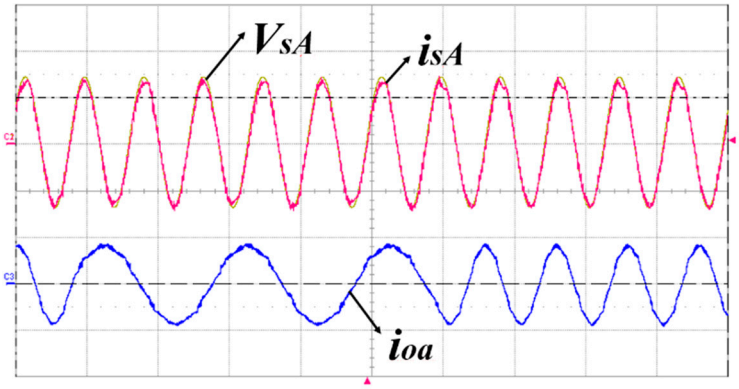

Figure 18. Experimental results of the proposed strategy with the IFRS, in which the reference of the output-current amplitude is 4 A and the reference of the output-current frequency is changed from 25 Hz to 50 Hz, x axis 20 ms/div. Waveforms of source voltage V_{sA} (100 V/div), source current i_{sA} (2 A/div) and output current i_{oa} (5 A/div).

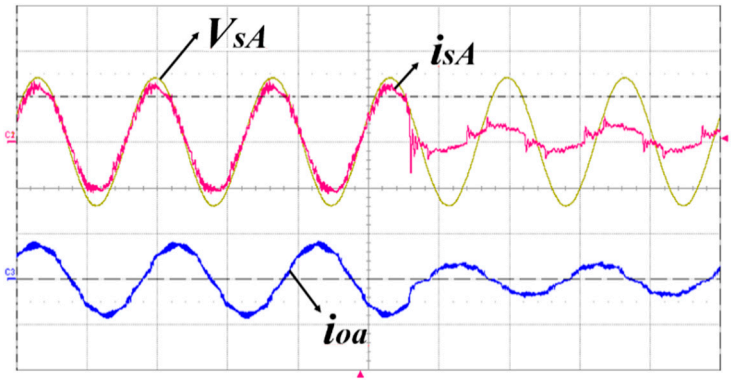

Figure 19. Experimental results of the proposed strategy with the IFRS, in which the reference of the output-current amplitude is changed from 4 A to 2 A and the reference of the output-current frequency is 50 Hz, x axis 10 ms/div. Waveforms of source voltage V_{sA} (100 V/div), source current i_{sA} (2 A/div) and output current i_{oa} (5 A/div).

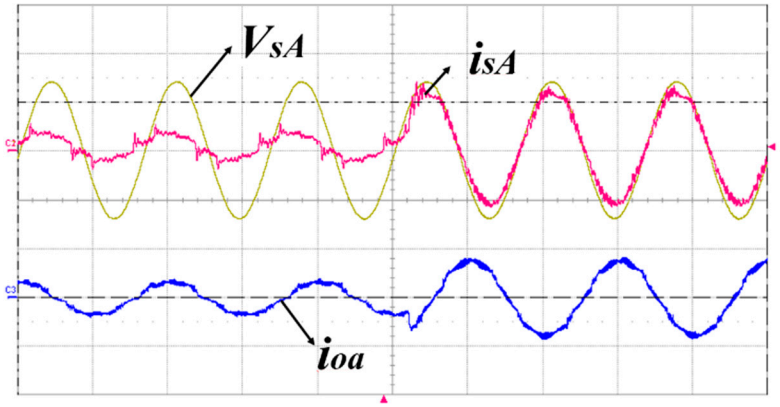

Figure 20. Experimental results of the proposed strategy with the IFRS, in which the reference of the output-current amplitude is changed from 2 A to 4 A and the reference of the output-current frequency is 50 Hz, x axis 10 ms/div. Waveforms of source voltage V_{sA} (100 V/div), source current i_{sA} (2 A/div) and output current i_{oa} (5 A/div).

7. Conclusions

An input filter is necessary for the commutation of switching devices and to mitigate against line-current harmonics. However, the filter configuration presents a resonance

frequency and can be excited by the utility due to the potential fifth and seventh harmonics in the ac source (series resonance) and also by the converter itself (parallel resonance). In addition, the input filter resonance is easier to be inspired by the model predictive control, when compared with traditional control methods, leading to additional harmonics in the AC source and distorted source current waveforms.

A vector modulation-based model predictive control strategy is proposed to solve these above problems, which controls the source reactive power and the output currents with fixed switching frequency. In addition, the advantage of the proposed VMMPCC strategy compared with the CMPC is firstly proved using the principle of vector synthesis and the law of sines in the vector distribution area. Besides, a zero-current switching sequence is proposed, which can guarantee safe zero-current switching operations and reduce the switching losses. This pattern can simplify the commutation of TSMC and avoid complex commutation strategies (e.g., four-step commutation) in traditional control methods. Furthermore, a novel input filter resonance suppression method is proposed and implemented in the VMMPCC for the TSMC, which shows good damping performance and easy implementation.

The performance of the proposed method is verified by simulation and experiment, which features unity input power factor, low source-current distortions, good sinusoidal waveforms of output currents and zero-current switching operations.

In addition, the CMPC only considers the optimal variable in one sampling instant, that is, it can achieve the optimal control effect in one sampling instant. However, it cannot guarantee the optimal control effects in the following sampling instants. The reason is that the CMPC ignores the optimal information that may be contained in other switching states, which may have negative effects on the control performance, such as divergence or oscillation. Therefore, it is necessary to expand the prediction time domain. In [38,39], the multi-step prediction methods are proposed which aims to obtain the optimal variables in multiple sampling instants. It should be a meaningful work to apply the multi-step predictive control to the TSMC in future.

Author Contributions: Conceptualization, methodology and validation, Z.D. and D.X.; formal analysis, investigation, resources and writing—original draft preparation, Z.D. and K.Z.; writing—review and editing, supervision and project administration, D.X.; funding acquisition, K.Z. All authors have read and agreed to the published version of the manuscript.

Funding: This work was supported in part by the Natural Science Basic Research Plan in Shaanxi Province of China under Grant 2018JM5033 and in part by the China Scholarship Council under Grant 201606290180.

Institutional Review Board Statement: Not applicable.

Informed Consent Statement: Not applicable.

Data Availability Statement: Data available on request due to restrictions eg privacy or ethical. The data presented in this study are available on request from the corresponding author. The data are not publicly available due to commercial sensitivity.

Acknowledgments: The authors thank the Natural Science Basic Research Plan in Shaanxi Province of China and the China Scholarship Council.

Conflicts of Interest: The authors declare no conflict of interest.

References

1. Friedli, T.; Kolar, J.W.; Rodriguez, J.; Wheeler, P.W. Comparative Evaluation of Three-Phase AC–AC Matrix Converter and Voltage DC-Link Back-to-Back Converter Systems. *IEEE Trans. Ind. Electron.* **2012**, *59*, 4487–4510. [CrossRef]
2. Wheeler, P.; Rodriguez, J.; Clare, J.; Empringham, L.; Weinstein, A. Matrix converters: A technology review. *IEEE Trans. Ind. Electron.* **2002**, *49*, 276–288. [CrossRef]
3. Alesina, A.; Venturini, M.G.B. Analysis and design of optimum-amplitude nine-switch direct AC-AC converters. *IEEE Trans. Power Electron.* **1989**, *4*, 101–112. [CrossRef]

4. Kolar, J.W.; Friedli, T.; Rodriguez, J.; Wheeler, P.W. Review of Three-Phase PWM AC–AC Converter Topologies. *IEEE Trans. Ind. Electron.* **2011**, *58*, 4988–5006. [CrossRef]
5. Lee, M.Y.; Wheeler, P.; Klumpner, C. Space-Vector Modulated Multilevel Matrix Converter. *IEEE Trans. Ind. Electron.* **2010**, *57*, 3385–3394. [CrossRef]
6. Lei, J.; Zhou, B.; Bian, J.; Qin, X.; Wei, J. A Simple Method for Sinusoidal Input Currents of Matrix Converter Under Unbalanced Input Voltages. *IEEE Trans. Power Electron.* **2015**, *31*, 21–25. [CrossRef]
7. Rivera, M.; Wheeler, P.; Olloqui, A.; Khaburi, D.A. A Review of Predictive Control Techniques for Matrix Converters—Part I. In Proceedings of the 2016 7th Power Electronics and Drive Systems Technologies Conference (PEDSTC), Tehran, Iran, 16–18 February 2016; Institute of Electrical and Electronics Engineers (IEEE): Newark, NJ, USA, 2016; pp. 582–588.
8. Rodriguez, J.; Rivera, M.; Kolar, J.W.; Wheeler, P.W. A Review of Control and Modulation Methods for Matrix Converters. *IEEE Trans. Ind. Electron.* **2012**, *59*, 58–70. [CrossRef]
9. Nguyen, T.; Lee, H.-H. A New SVM Method for an Indirect Matrix Converter with Common-Mode Voltage Reduction. *IEEE Trans. Ind. Inform.* **2014**, *10*, 61–72. [CrossRef]
10. Sun, Y.; Li, X.; Su, M.; Wang, H.; Dan, H.; Xiong, W. Indirect Matrix Converter-Based Topology and Modulation Schemes for Enhancing Input Reactive Power Capability. *IEEE Trans. Power Electron.* **2015**, *30*, 4669–4681. [CrossRef]
11. Tsoupos, A.; Khadkikar, V.M. A Novel SVM Technique with Enhanced Output Voltage Quality for Indirect Matrix Converters. *IEEE Trans. Ind. Electron.* **2018**, *66*, 832–841. [CrossRef]
12. Rivera, M.; Rojas, C.; Wilson, A.; Rodriguez, J.; Espinoza, J.; Baier, C.; Muñoz, J. Review of predictive control methods to improve the input current of an indirect matrix converter. *IET Power Electron.* **2014**, *7*, 886–894. [CrossRef]
13. Ahmed, A.A.; Koh, B.K.; Lee, Y.I. A Comparison of Finite Control Set and Continuous Control Set Model Predictive Control Schemes for Speed Control of Induction Motors. *IEEE Trans. Ind. Inform.* **2018**, *14*, 1334–1346. [CrossRef]
14. Formentini, A.; Trentin, A.; Marchesoni, M.; Zanchetta, P.; Wheeler, P. Speed Finite Control Set Model Predictive Control of a PMSM Fed by Matrix Converter. *IEEE Trans. Ind. Electron.* **2015**, *62*, 6786–6796. [CrossRef]
15. Gulbudak, O.; Santi, E. FPGA-Based Model Predictive Controller for Direct Matrix Converter. *IEEE Trans. Ind. Electron.* **2016**, *63*, 4560–4570. [CrossRef]
16. Siami, M.; Khaburi, D.A.; Rodriguez, J. Simplified Finite Control Set-Model Predictive Control for Matrix Converter-Fed PMSM Drives. *IEEE Trans. Power Electron.* **2017**, *33*, 2438–2446. [CrossRef]
17. Rivera, M.; Yaramasu, V.; Llor, A.; Rodriguez, J.; Wu, B.; Fadel, M. Digital Predictive Current Control of a Three-Phase Four-Leg Inverter. *IEEE Trans. Ind. Electron.* **2013**, *60*, 4903–4912. [CrossRef]
18. Tarisciotti, L.; Zanchetta, P.; Watson, A.; Wheeler, P.W.; Clare, J.C.; Bifaretti, S. Multiobjective Modulated Model Predictive Control for a Multilevel Solid-State Transformer. *IEEE Trans. Ind. Appl.* **2015**, *51*, 4051–4060. [CrossRef]
19. Vijayagopal, M.; Empringham, L.; de Lillo, L.; Tarisciotti, L.; Zanchetta, P.; Wheeler, P. Control of a Direct Matrix Converter Induction Motor Drive with Modulated Model Predictive Control. In Proceedings of the 2015 IEEE Energy Conversion Congress and Exposition (ECCE), Montreal, QC, Canada, 20–24 September 2015; Institute of Electrical and Electronics Engineers (IEEE): Newark, NJ, USA, 2015; pp. 4315–4321.
20. Vijayagopal, M.; Zanchetta, P.; Empringham, L.; de Lillo, L.; Tarisciotti, L.; Wheeler, P. Control of a Direct Matrix Converter with Modulated Model-Predictive Control. *IEEE Trans. Ind. Appl.* **2017**, *53*, 2342–2349. [CrossRef]
21. Renault, A.; Ayala, M.; Comparatore, L.; Pacher, J.; Gregor, R. Comparative Study of Predictive-Fixed Switching Techniques for a Cascaded H-Bridge Two level STATCOM. In Proceedings of the 2018 53rd International Universities Power Engineering Conference (UPEC), Glasgow, Scotland, 4–7 September 2018; Institute of Electrical and Electronics Engineers (IEEE): Newark, NJ, USA, 4 September 2018; pp. 1–6.
22. Garcia, C.F.; Silva, C.A.; Rodriguez, J.R.; Zanchetta, P.; Odhano, S.A. Modulated Model-Predictive Control with Optimized Overmodulation. *IEEE J. Emerg. Sel. Top. Power Electron.* **2019**, *7*, 404–413. [CrossRef]
23. He, Z.; Guo, P.; Shuai, Z.; Xu, Q.; Luo, A.; Guerrero, J.M. Modulated Model Predictive Control for Modular Multilevel AC/AC Converter. *IEEE Trans. Power Electron.* **2019**, *34*, 10359–10372. [CrossRef]
24. Fang, F.; Tian, H.; Li, Y. Finite Control Set Model Predictive Control for AC–DC Matrix Converter with Virtual Space Vectors. *IEEE J. Emerg. Sel. Top. Power Electron.* **2021**, *9*, 616–628. [CrossRef]
25. Di, Z.; Rivera, M.; Dan, H.; Tarisciotti, L.; Zhang, K.; Xu, D.; Wheeler, P. Modulated model predictive current control of an indirect matrix converter with active damping. In Proceedings of the IECON 2017—43rd Annual Conference of the IEEE Industrial Electronics Society, Beijing, China, 29 October–1 November 2017; Institute of Electrical and Electronics Engineers (IEEE): Newark, NJ, USA, 2017; pp. 1313–1318.
26. Wang, F.; Chen, N.; Xia, A.; Rodriguez, J. Modulated Model Predictive Control of Two-Stage Matrix Converter for Reducing Common-mode Voltage. In Proceedings of the IEEE International Symposium on Predictive Control of Electrical Drives and Power Electronics (PRECEDE 2019), Quanzhou, China, 31 May–2 June 2019; Institute of Electrical and Electronics Engineers (IEEE): Newark, NJ, USA, 4 July 2019. [CrossRef]
27. Salo, M.; Tuusa, H. A vector controlled current-source PWM rectifier with a novel current damping method. *IEEE Trans. Power Electron.* **2000**, *15*, 464–470. [CrossRef]
28. Sun, Y.; Su, M.; Li, X.; Wang, H.; Gui, W. A General Constructive Approach to Matrix Converter Stabilization. *IEEE Trans. Power Electron.* **2013**, *28*, 418–431. [CrossRef]

29. Sato, I.; Itoh, J.-I.; Ohguchi, H.; Odaka, A.; Mine, H. An Improvement Method of Matrix Converter Drives Under Input Voltage Disturbances. *IEEE Trans. Power Electron.* **2007**, *22*, 132–138. [CrossRef]
30. Mariethoz, S.; Morari, M. Explicit Model-Predictive Control of a PWM Inverter with an LCL Filter. *IEEE Trans. Ind. Electron.* **2008**, *56*, 389–399. [CrossRef]
31. Lei, J.; Zhou, B.; Qin, X.; Wei, J.; Bian, J. Active damping control strategy of matrix converter via modifying input reference currents. *IEEE Trans. Power Electron.* **2015**, *30*, 5260–5271. [CrossRef]
32. Rivera, M.; Rodriguez, J.; Wu, B.; Espinoza, J.R.; Rojas, C.A. Current Control for an Indirect Matrix Converter with Filter Resonance Mitigation. *IEEE Trans. Ind. Electron.* **2011**, *59*, 71–79. [CrossRef]
33. Rivera, M.; Rojas, C.; Rodríguez, J.; Wheeler, P.; Wu, B.; Espinoza, J. Predictive Current Control with Input Filter Resonance Mitigation for a Direct Matrix Converter. *IEEE Trans. Power Electron.* **2011**, *26*, 2794–2803. [CrossRef]
34. Akagi, H.; Watanabe, E.; Aredes, M. More power to you (review of Instantaneous Power Theory and Applications to Power Conditioning by Akagi, H. et al.; 2007) [book review]. *IEEE Power Energy Mag.* **2007**, *6*, 80–81. [CrossRef]
35. Wang, X.; Lin, H.; Feng, B.; Lyu, Y. Damping of Input LC Filter Resonance Based on Virtual Resistor for Matrix Converter. In Proceedings of the 2012 IEEE Energy Conversion Congress and Exposition (ECCE), Raleigh, NC, USA, 15–20 September 2012; pp. 3910–3916. [CrossRef]
36. Trentin, A.; Empringham, L.; de Lillo, L.; Zanchetta, P.; Wheeler, P.; Clare, J. Experimental Efficiency Comparison Between a Direct Matrix Converter and an Indirect Matrix Converter Using Both Si IGBTs and SiC mosfets. *IEEE Trans. Ind. Appl.* **2016**, *52*, 4135–4145. [CrossRef]
37. Zhang, X.; Zhang, L.; Zhang, Y. Model Predictive Current Control for PMSM Drives with Parameter Robustness Improvement. *IEEE Trans. Power Electron.* **2019**, *34*, 1645–1657. [CrossRef]
38. Gulbudak, O.; Gokdag, M. Asymmetrical Multi-Step Direct Model Predictive Control of Nine-Switch Inverter for Dual-Output Mode Operation. *IEEE Access* **2019**, *7*, 164720–164733. [CrossRef]
39. Yu, Y.; Wang, X. Multi-Step Predictive Current Control for NPC Grid-Connected Inverter. *IEEE Access* **2019**, *7*, 157756–157765. [CrossRef]